Computational Materials Science 153 (2018) 438–444

Contents lists available at ScienceDirect

Computational Materials Science

journal homepage: www.elsevier.com/locate/commatsci

First principles study of the electronic properties and Schottky barrier in vertically stacked graphene on the Janus MoSeS under electric field

Khang D. Pham[a,b], Nguyen N. Hieu[c], Huynh V. Phuc[d], Bui D. Hoi[e], Victor V. Ilysov[f], Bin Amin[g], Chuong V. Nguyen[h,*]

[a] Theoretical Physics Research Group, Advanced Institute of Materials Science, Ton Duc Thang University, Ho Chi Minh City, Viet Nam
[b] Faculty of Applied Sciences, Ton Duc Thang University, Ho Chi Minh City, Viet Nam
[c] Institute of Research and Development, Duy Tan University, Da Nang, Viet Nam
[d] Division of Theoretical Physics, Dong Thap University, Dong Thap, Viet Nam
[e] Physics Department, University of Education, Hue University, Hue, Viet Nam
[f] Department of Physics, Don State Technical University, Rostov on Don, Russia
[g] Department of Physics, Haraza Universtiy, Mansehra 21300, Pakistan
[h] Department of Materials Science and Engineering, Le Quy Don Technical University, Ha Noi, Viet Nam

A R T I C L E I N F O

Keywords:
Graphene
Janus MoSeS
Electronic properties
Schottky contact
Electric field

A B S T R A C T

In this paper, we design novel ultra-thin graphene/MoSeS and graphene/MoSSe heterostructures and investigate systematically their structural and electronic properties as well as the effect due to perpendicularly applied electric field on the heterostructure. Our results show that the electronic properties of both the graphene (Gr) and Janus MoSeS monolayer are well kept in the Gr/MoSeS and Gr/MoSSe heterostructures due to weak interaction between them. The interlayer distance between the Gr and Janus MoSeS monolayer is derived to be 3.34 Å, whereas the binding energy in the heterostructure is found to be −3 meV per carbon atom, indicating the weak interactions between the Gr and Janus MoSeS layers. We find that in both Gr/MoSeS and Gr/MoSSe heterostructures, the Gr becomes a semiconductor with a tiny band gap of about 3 meV, forming between the π and π^* bands at the high symmetry K point. The appearance of the fundamental band gap in the Gr makes it suitable for application in electronics and optoelectronics like as field effect transistors. Furthermore, the Gr/MoSeS heterostructure forms an n-type Schottky contact with the Schottky barrier height of 0.53 eV at the equilibrium state. Our results also indicate that the electric field applied perpendicularly to the heterostructure could control not only the Schottky barrier height, but also the Schottky contact type from the n-type to p-type. Based on these extraordinary electronic properties of ultra-thin Gr/MoSeS heterostructures, which are expected to be with applications in nanoelectronic and optoelectronic devices in the future experiments.

1. Introduction

Two-dimensional (2D) materials have recently gained significant interest in the research community due to their unique properties and wide potential applications in nanoelectronics and optoelectronics. The popular 2D materials, such as graphene (G) [1,2], hexagonal boron nitride (h-BN) [3–5], transition metal dichalcogenides (TMDs) [6–10], single-layer post-transition-metal chalcogenides (PTMCs) [11–15] have attracted much interest recently. Among these, graphene has been studied widely owing to its extraordinary properties, such as high carrier mobility and massless Dirac fermions. However, the lack of a tiny band gap around the Dirac point of graphene limits its applications for nanoelectronic and optoelectronic devices. To get around the limit, it is required to modify the electronic properties, especially the band gap of graphene. To date, there are many common way, which can be used to open a tiny band gap in graphene, namely strain engineering, electric field, substrates, and substitutional doping. It is clear both experimentally and theoretically that under these external conditions, the graphene becomes a semiconductor with a tiny band gap of about a few tens up to a few hundreds meV, which makes it suitable for numerous nanoelectronic and optoelectronic applications.

Very recently, a structurally stable Janus MoSSe monolayer has been successfully synthesized by breaking the out-of-plane structural symmetry of MoS_2 monolayer [16] or by a controlled sulfurization process based on a $MoSe_2$ monolayer [17]. Interestingly, each unit cell of the Janus MoSSe monolayer consists of three atoms, in which one

* Corresponding author.
E-mail addresses: phamdinhkhang@tdt.edu.vn (K.D. Pham), chuong.vnguyen@lqdtu.edu.vn (C.V. Nguyen).

https://doi.org/10.1016/j.commatsci.2018.07.017
Received 24 May 2018; Accepted 9 July 2018
0927-0256/ © 2018 Elsevier B.V. All rights reserved.

side is Se atom, the other side is S atom, and the Mo atom is sandwiched between S and Se atomic layers. The crystal of the Janus MoSSe monolayer differs from those of perfect MoS_2 and $MoSe_2$ monolayers. This may lead to many new superior properties that MoS_2 or $MoSe_2$ do exhibit. For example, due to the lack of the reflection symmetry, the Janus MoSeS monolayer has large in-plane and vertical piezoelectric effect, making it a great material for nanoscale electronic and energy applications [18]. Moreover, owing to the difference in the electronegativity between Se and S atoms, the Janus MoSeS monolayer has an intrinsic moment, resulting in the separation of holes and electrons causing enhanced photocatalytic activity [19]. The electronic and optical properties of the pristine Janus MoSeS monolayer has recently been investigated by means of the first principles calculations based on the density functional theory (DFT) [20], which could bring exciting novel properties and great potential in nanoelectronic and optoelectronic devices. The effect of a biaxial strain on the electronic properties and the power factor in Janus MoSeS monolayer have also been theoretically investigated [21,22]. These studies show that the electronic properties of the Janus MoSeS monolayer are very sensitive to the biaxial strain. It is found that the lattice thermal conductivity of the Janus MoSSe monolayer is lower than that of the MoS_2 monolayer, but is higher than that of the $MoSe_2$ monolayer [21]. It is well known that the Janus MoSeS monolayer is a direct semiconductor with the band gap of 1.56 eV, 2.03 eV, and 2.64 eV, respectively by using PBE, HSE06, and G_0W_0 functionals [20].

Currently, G-based heterostructures combining the G layer and other 2D semiconducting layer have received considerable interest, both experimentally and theoretically, owing to their extraordinary properties [23–27]. More interestingly, various electronic devices based on the G-vdW heterostructures have been recently successfully fabricated. Examples are, G/GaSe dual Schottky diode [27], and photodetector [26], G/MoS_2 gas sensor [28], field-effect Schottky barrier transistor [29], and hybrid phototransistor [30], G/WS_2 field effect transistor [31], and so on. These findings suggest the opportunities of the vdW G-based heterostructures in the next-generation electronics, which can replace the principal silicon-based devices. Concurrently, the structural and electronic properties and Schottky contact of many G-based vdW heterostructures, especially G/TMDs heterostructures, such as G/MoS_2 [32–36], G/$MoSe_2$ [23,37,38], G/WS_2 [24,39,40] and G/WSe_2 [41–43] heterostructures, have also been investigated both experimentally and theoretically. However, up to date the structural and electronic properties of the combination between G and Janus MoSeS monolayer have not yet been studied systematically.

Therefore, in this paper, for the first time we design new ultrathin G/MoSeS and G/MoSSe heterostructures and investigate theoretically their structural, electronic properties and Schottky contact, as well as the effect of an electric field applied perpendicularly to the heterostructure surface on their electronic properties and Schottky barrier height by means of the density functional theory from first-principles calculations. The results show that, owing to the weak vdW interactions between the G layer and Janus MoSeS monolayer, the intrinsic electronic properties of the G/MoSeS and G/MoSSe heterostructures well preserve those of freestanding G and Janus MoSeS monolayer. We also find that both the G/MoSeS and G/MoSSe heterostructures form an *n*-type Schottky contact. Furthermore, our calculations also indicate that an external electric field applied perpendicularly to the heterostructure surface could control both the Schottky barrier height and Schottky contacts (*n*-type and *p*-type). Our findings show an opportunity for the G/MoSeS heterostructure in the next-generation electronics to replace principal silicon-based devices.

2. Computational methodology

In this work, all calculations were performed within the density functional theory (DFT), which is implemented in the Quantum Espresso simulation package [44]. In order to describe the exchange-correlation energy we used the generalized gradient approximation (GGA) [45,46] of Perdew, Burke, and Ernzerhof (PBE) [47]. In order to describe the electron–ion potential, we used the projected augmented wave (PAW) potential [48]. The kinetic cut-off energy is set to 500 eV for the plane wave expansion. The first Brillouin zone (BZ) sampling of $12 \times 12 \times 1$ Monkhorst–Pack *k*–point grid is used to perform geometric optimization, whereas the BZ sampling of $9 \times 9 \times 1$ *k*-point grid is used to perform all the electronic properties calculations. In order to describe the non-bonding interactions, the DFT-D2 method proposed by Grimme (DFT-D2) [49] was adopted. In DFT-D2 approximation, the vdW interaction was described by adding a semi-empirical dispersion potentials to the conventional DFT energy. In addition, a large vacuum region of 20 Å is used to avoid artificial interactions with spurious replica images. All geometric structures are fully relaxed until energy and forces are converging to 10^{-6} eV and 0.001 eV/Å, respectively.

3. Results and discussion

3.1. Structural and electronic properties of Janus MoSeS monolayer

Before designing and considering the G/MoSeS and G/MoSSe heterostructures, we first investigate the structural and electronic properties of a single-layer Janus MoSeS crystal at the equilibrium state. Our calculated lattice parameter of the Janus MoSeS after full relaxation is $a = 3.218$ Å, that is in good agreement with previous results. It can be seen that each Janus MoSeS unit cell consists of three atomic layers, composing of Mo layer sandwiched between the S and Se layers. The corresponding Mo–Se and Mo–S bond lengths in the Junus monolayer MoSeS at the equilibrium state are 2.51 Å and 2.41 Å, respectively. In addition, the vertical thicknesses of Mo–Se (Δ), and Se–S (h) are 1.72 Å, and 3.23 Å, respectively. It can be seen that these vertical thicknesses are shorter than that of the MoS_2 monolayer, but longer than that of the $MoSe_2$ monolayer, resulting in a break of structure symmetry in the vertical plane. The nature of such a break is due to the difference in atomic sizes and electronegativities of Se and S atoms in the Janus MoSeS monolayer.

Fig. 1(a) shows the electronic band structures and partial density of states (PDOS) for the corresponding MoS_2, $MoSe_2$ and Janus MoSeS monolayers at the equilibrium state. One can observe first that all three MoS_2, $MoSe_2$ and Janus MoSeS monolayers are semiconductors with the corresponding band gaps of 1.70 eV, 1.52 eV, and 1.49 eV, respectively. These results are in good agreement with previous values [20]. The direct band gap of Janus MoSeS monolayer is contributed by the valence band maximum (VBM) and the conduction band minimum (CBM) at the high symmetry K point. Thus the electrons are photo-excited from the VBM to the CBM directly, making Janus MoSeS monolayer suitable for the generation of photo-excited electrons and holes Fig. 1(b).

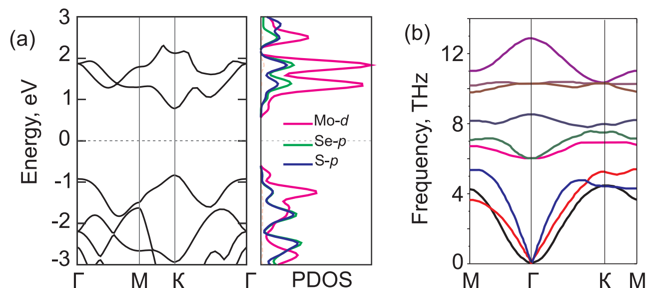

Fig. 1. (a) Calculated band structures and partial density of states of Janus MoSeS monolayer at the equilibrium state. The Fermi level is set to be zero. (b) Phonon dispersion curves of Janus MoSeS monolayer at equilibrium state.

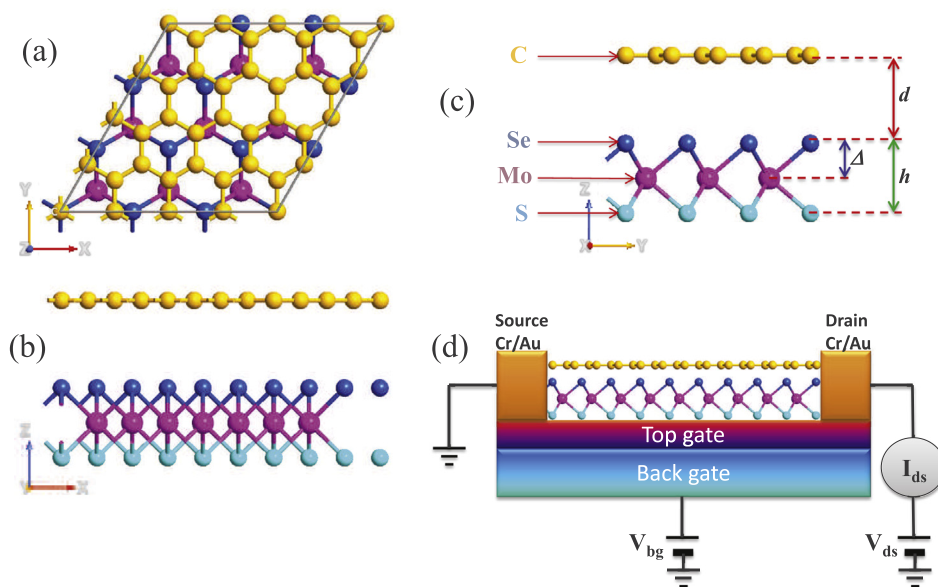

Fig. 2. (a) Top view, (b, c) side views of the relaxed geometric structure of G/MoSeS heterostructure.

3.2. Electronic properties and Schottky contact in graphene stacked on Janus MoSeS monolayer

We now consider the structural and electronic properties of the G layer stacked on the Janus MoSeS monolayer in its two different stacking configurations, as shown in Fig. 2. In these heterostructures, one Se(S) atom is located directly on one C atom, and another Se(S) atom located on the center of hexagonal C ring atoms. In the first stacking configuration, the G layer is stacked on the topmost Se layer of the Janus MoSeS monolayer, namely G/MoSeS heterostructure, whereas in the other configuration called G/MoSSe heterostructure, the G layer is stacked on the topmost S layer. The lattice parameter between the G layer and Janus MoSeS monolayer is larger than 20%. Additionally, it also should be noted that the electronic properties of the Janus MoSeS are sensitive to the strain [22]. Thus, in order to combine the G layer and the Janus MoSeS monolayer, we choose to keep the lattice parameter of Janus MoSeS monolayer and fix the lattice parameter of the G. Moreover, (4 × 4) cells of G is used to match (3 × 3) cells of Janus MoSeS monolayer. Our calculated lattice parameter of G/MoSeS heterostructure is 9.66 Å, indicating a small lattice mismatch of about 2%. After full relaxation, the interlayer distance between the G layer and the topmost Se layer in the G/MoSeS heterostructure is 3.34 Å, and between the G and the topmost S layer in the G/MoSSe heterostructure is 3.45 Å. We find that these interlayer distances are the same as those in other vdW heterostructures, such as G/WSe_2 [50], G/GaN [51], G/MoS_2 [32,33,36], and so on. Moreover, after the relaxation, one can observe that both the Mo–Se (Δ) and Se–S (*h*) thicknesses are decreased from 1.72 Å and 3.23 Å to 1.68 Å and 3.19 Å, respectively.

In order to determine the stability of G/MoSeS heterostructure, we calculate the binding energy per carbon atom as follows: $E_b = [E_{HS} - E_G - E_{MoSeS}]/n$. Here, E_{HS}, E_G, and E_{MoSeS} are, respectively, the corresponding total energy of the heterostructure, the freestanding G, and the Janus MoSeS monolayer, whereas n is the number of carbon atoms in the calculated heterostructure. Our calculated binding energy per carbon atom for the corresponding G/MoSeS and G/MoSSe heterostructures is −3.51 meV and −3.05 meV. These values for the binding energies indicate that G/MoSeS and G/MoSSe heterostructures considered here are both stable at the equilibrium state. Moreover, it can be seen that these binding energies have the same magnitude as the binding energies per carbon atom in other vdW graphene-based heterostructures. Ma et al., for instance, have indicated that the binding energy per carbon atom in the G/MoS_2 and G/$MoSe_2$ heterostructures are −23 meV [32] and −21 meV [37], respectively. They showed that in all different stacking configurations of G/MoS_2 and G/$MoSe_2$ heterostructures, graphene was found to interact very weakly with both the MoS_2 and $MoSe_2$ monolayers. Zhang and co-workers have found that the G at the equilibrium state is bound to WS_2 monolayer in the G/WS_2 heterostructure *via* very weak vdW interaction, with the interlayer distance of 3.49 Å, and the binding energy of −26.8 meV per carbon atom. According to these results, it can be observed that both the G/MoSeS and G/MoSSe heterostructures are characterized by the weak vdW interactions between the G and the MoSeS monolayer.

We next focus on the electronic properties of both G/MoSeS and G/MoSSe heterostructures as shown in Fig. 3(c) and (d). In order to better understand the electronic properties of the heterostructure, we calculate the band structures, partial density of states (PDOS), and total density of states (TDOS) of (4 × 4) supercell of the G layer and (3 × 3) supercell of the Janus MoSeS monolayer. First, one can observe that freestanding graphene has a zero band gap, forming a linear Dirac-like dispersion around the Fermi level. Secondly, we find that (3 × 3) supercells of the Janus MoSeS monolayer shows a direct semiconductor with the band gap of 1.51 eV, forming between the VBM and CBM located at the *K* point, as shown in Fig. 3(b). It means that the band gap of the (4 × 4) isolated Janus MoSeS monolayer is smaller than that of an unit cell Janus MoSeS monolayer by 0.01 eV. Moreover, the Fermi level of the isolated (3 × 3) Janus MoSeS monolayer shifts upward from the VBM to CBM as compared with (1 × 1) Janus MoSeS monolayer. The position of the VBM and CBM should be also noted: in comparison with the band structure of Janus MoSeS monolayer primitive cell, the VBM and the CBM of Janus MoSeS monolayer in (3 × 3) supercell are folded from high symmetry *K* point to another one (Γ point). This band folding was also observed in the (3 × 3) supercell of WSe_2 monolayer [50] and WS_2 monolayer [24].

Fig. 3(c) and (d) shows the projected band structures of G/MoSeS and G/MoSSe heterostructures at the equilibrium interlayer distance. Due to the weak vdW interaction between the G and Janus MoSeS monolayer, the projected band structures of both G/MoSeS and G/MoSSe heterostructures look just like the sum of the band structures of freestanding G and the isolated Janus MoSeS monolayer. It means that the extraordinary electronic properties of both graphene and Janus MoSeS monolayer are well preserved in those heterostructures. Compared with the band structure of freestanding graphene, we find that a tiny band gap, about 3 meV and 2 meV, respectively, is opened at the

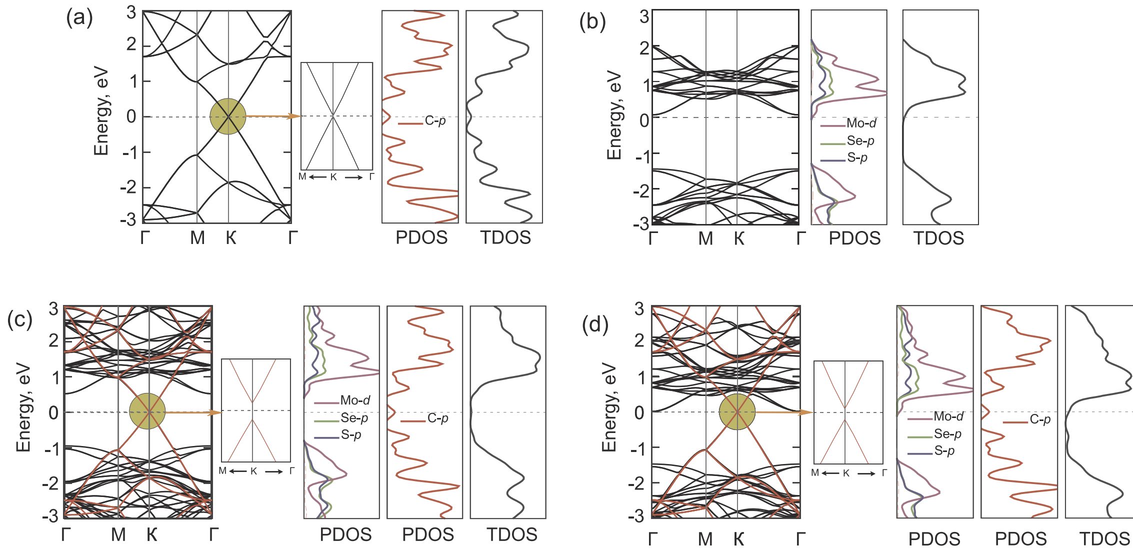

Fig. 3. Calculated band structures, PDOS and total DOS of (a) (4 × 4) supercell of freestanding graphene, (b) (3 × 3) supercell of Janus MoSeS monolayer, (c) G/MoSeS heterostructure and (d) G/MoSSe heterostructure. The Fermi level is set to be zero.

Dirac point of graphene at the G/MoSeS and G/MoSSe heterostructures, as shown in the insets of Fig. 3(c) and (d). Thus, the G becomes a semiconductor with a tiny band gap, forming between the π and π^* bands at the high symmetry K point. The appearance of the fundamental band gap in the G makes it suitable for application in electronics and optoelectronics, such as FETs. A tiny opening band gap in the G also suggests that the electron mobility in the considered heterostructures is almost unchanged from that in the freestanding G. This finding indicates that the Janus MoSeS monolayer can be considered as a potential substrate for designing graphene-based vdW heterostructures. The nature of band gap opening in the G is due to a symmetry breaking of the sublattices A and B for two carbon atoms in each graphene unit cell. In order to better understand the physical mechanism of the band gap opening in our G/MoSeS and G/MoSSe heterostructures, we use the tight-binding (TB) model analysis, in which the linear dispersion around Fermi level of graphene can be calculated as follows: $E(k) = \sqrt{\Delta^2 \pm (\hbar v_F k)^2}$, where k is the wave vector relative to the Dirac point, v_F is the Fermi velocity, and Δ is the on-site energy difference between the two A and B sub-lattices of the G. The $\pm$ signs correspond to conduction bands and valence bands, respectively. For the freestanding G, the on-site energies of the two A and B sub-lattices are identical ($\Delta = 0$), resulting in the zero band gap and the linear dispersion relation near the Dirac point. For the G/MoSeS and G/MoSSe herostructures, the charge redistribution breaks the equivalence of the two graphene sub-lattices, giving rise to a non zero band gap, $E_g = 2\Delta$.

It should be noted that in order to design novel high-performance nanoelectronic devices based on these G/MoSeS and G/MoSSe heterostructures, it is required to maintain graphene's high carrier mobility in these heterostructures. It is well known that the effective mass for electrons (m_e^*) and holes (m_h^*) of graphene is closely related to its carrier mobility as $\mu = e\tau/m^*$. Therefore, in order to estimate the carrier mobility of the heterostructure, we further calculate its effective mass. The effective mass of electron/hole is calculated by fitting parabolic functions to the VBM and CBM of the heterostructure for the wave vector as follows: $m^* = \hbar(\partial^2 E(k)/\partial k^2)^{-1}$. Here, k is wave vector and $\hbar$ is Planck's constant. At the equivalent interlayer distance, the effective mass for electrons and holes at the Γ Dirac point for the G/MoSeS heterostructure is very small of 1.17×10^{-2} m_0, and 1.28×10^{-2} m_0, respectively. These small effective masses for electrons and holes indicate that considered heterostructures here can maintain a high carrier mobility, which makes them suitable material for application in high speed nanoelectronic and optoelectronic devices.

As mentioned above, both the G/MoSeS and G/MoSSe heterostructures show a metal–semiconductor contact, formed between the metallic G and semiconductor Janus MoSeS monolayer. We find that a Schottky contact can be observed in these metal-semiconductor heterostructures. Based on the Schottky-Mott model [52] at the metal/semiconductor heterostructures [53], an n-type Schottky barrier is defined as the energy difference between the Fermi level (E_F) and the conduction band minimum (E_{CBM}), $\Phi_{Bn} = E_{CBM} - E_F$. Similarly, a p-type Schottky barrier is defined as the energy difference between the Fermi level (E_F) and the valence band maximum (E_{VBM}), $\Phi_{Bp} = E_F - E_{VBM}$. Note that the sum of the n-type and the p-type Schottky barriers is approximately equal to the band gap of the semiconductor, that is $\Phi_{Bn} + \Phi_{Bp} \approx E_G$. It is well known that the Schottky barrier height (SBH) of the metal-semiconductor heterostructure affects strongly on the current flow. Thus, it is necessary to know the SBH of both the G/MoSeS and G/MoSSe heterostructures. We find that an n-type Schottky contact is formed in both the G/MoSeS and G/MoSSe heterostructures. Our calculated n-type SBH in the G/MoSeS and G/MoSSe heterostructures are 0.53 eV and 0.07 eV, respectively. It should be noted that the band gap and the SBH of the metal-semiconductor heterostructures could be controlled by applying electric field perpendicular to its surface or by varying its interlayer distance [24,54–57]. For example, Hu and coworkers [54] have indicated that by applying electric field and varying interlayer distance, one can control the n-type Schottky barrier height of the G/MoS_2 heterostructure. Moreover, they have found the transformation of Schottky contact from the n-type to p-type when the applied positive electric field is larger than 0.6 V/Å. This transition was also observed in the G/WS_2 heterostructure with electric field applied perpendicularly to the surface [24]. Furthermore, our previous calculations on the G/MoS_2 and G/GaSe heterostructures also indicate that their electronic properties and Schottky barrier could be modulated by an out-of-plane strain and electric field [36,57,58]. Therefore, we believe that the electronic properties, such as band gap opening and Schottky barrier in the G/MoSeS and G/MoSSe heterostructures, also could be controlled by applying electric field perpendicular to the surface or by changing the interlayer distance between the G and the nearest-neighbor layer of Janus MoSeS monolayer. The transition from the n-type to p-type Schottky contact plays an important role in designing a new generation of graphene-based electronic Schottky devices.

In Fig. 4 we present the electrostatic potential along the z direction of the G/MoSeS and G/MoSSe heterostructures. One can clearly observe

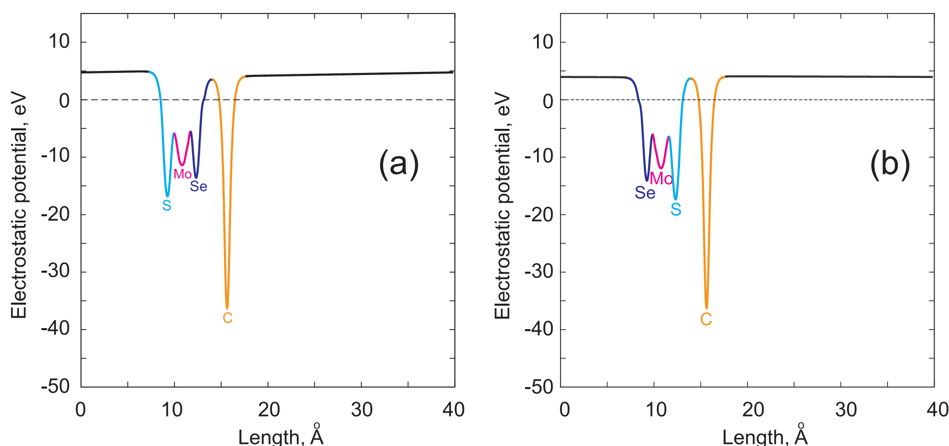

Fig. 4. The electrostatic potential of (a) G/MoSeS heterostructure and (b) G/MoSSe heterostructure along the z direction.

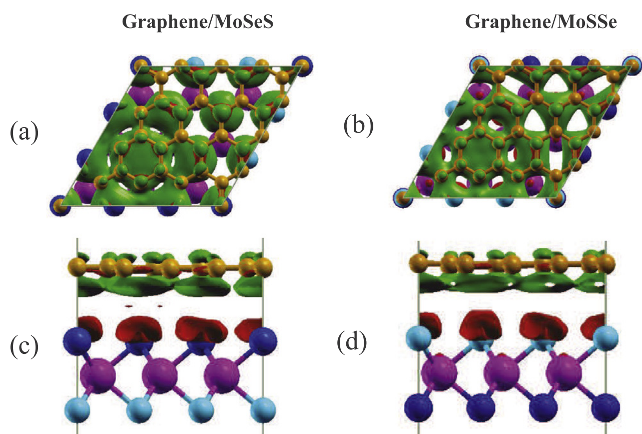

Fig. 5. Top view (a, b) and side view (c, d) of the charge density difference of G/MoSeS and G/MoSSe heterostructures at the equilibrium state with the isovalue of 10^{-4} eV/Å. Red and green isosurfaces correspond to the accumulation and depletion of electronic densities. (For interpretation of the references to color in this figure legend, the reader is referred to the web version of this article.)

that in both the G/MoSeS and G/MoSSe heterostructures, the G layer has a deeper electrostatic potential than that of the Janus MoSeS monolayer. The calculated difference in electrostatic potential between the G and the Janus MoSeS monolayer is very large, about 20 eV, across the heterostructure surface. This large potential drop (the difference in electrostatic potential between graphene and Janus MoSeS monolayer) indicates strong electrostatic field across the heterostructures, and thus may considerably impact the carrier dynamics and charge injection in the heterostructures. Although the interaction between the G layer and the Janus MoSeS and MoSSe monolayers in the considered heterostructures here is the weak vdW interaction, however, the charge density can be redistributed in the G/MoSeS and G/MoSSe heterostructures, forming an interface dipole. Notice that an interface dipole formed by the charge redistribution can shift the electronic levels from their original positions, leading to a deviation from the Schottky-Mott limit [59–61]. Thus, it is necessary to understand the mechanism of the charge distribution and charge transfer between the G layer and the Janus MoSeS (MoSSe) monolayer, which can be visualized by the charge density difference (CDD), as shown in Fig. 5. The charge density difference in these heterostructures can be calculated as follows: $\Delta\rho = \rho_{hetero} - \rho_G - \rho_{Janus}$, where ρ_{hetero}, ρ_G, and ρ_{Janus} are the charge densities of the corresponding heterostructure, freestanding graphene, and isolated Janus MoSeS monolayer, respectively. One can observe that the charge is transferred from the G layer to the Janus crystal in both stacking configurations of the heterostructures at the equilibrium state. Moreover, the charge density is redistributed in the G/MoSeS and G/MoSSe heterostructures, resulting in a formation of the electron-rich and hole-rich regions. Furthermore, the charge is depleted in the graphene layer and accumulated in the topmost of the Janus MoSeS and MoSSe layer, indicating that the charge transferred from the G layer to the Janus layer.

We next try to explore the effect of electric field (E_{field}) on the electronic properties and Schottky barrier of the G/MoSeS heterostructure. Recently, to improve the performance of the G-based electronic devices, it is common to use electric field. Thus, it is necessary to study the effect of the E_{field} on the physical properties of graphene-based heterostructure. In the present study, an electric field is applied perpendicularly to the heterostructure surface along the z direction, as shown in Fig. 6(a). Note that the direction of the E_{field} from the graphene layer to the Janus MoSeS monolayer is defined as the positive direction. We find that a positive electric field more than 1.5 V/nm can induce the transformation of the Schottky contact of the G/MoSeS heterostructure from the n-type to the p-type. On the other hand, the G/MoSeS heterostructure keeps an n-type Schottky contact under with negative applied electric field. The dependence of the SBH of the G/MoSeS heterostructure on the strength of the electric field is illustrated in Fig. 6(b). One can clearly observe that with increasing the strength of an electric field the n-type SBH increases linearly, whereas the p-type SBH decreases. The n-type SBH of the G/MoSeS heterostructure increases from 0.31 eV to 0.53 eV and then to 0.75 eV with the increasing strength of the electric field from −1.5 eV/nm to 0 V/nm and then to +1.5 V/nm, respectively, whereas the p-type SBH decreases from 1.16 eV to 0.94 eV and then to 0.72 eV. It can be seen that when the strength of the applied electric field is larger than +1.5 V/nm, the n-type SBH is larger than that of the p-type, resulting in a transition of the Schottky contact from the n-type to the p-type. It indicates that an electric field applied perpendicularly to the G/MoSeS heterostructure could control not only the SBH but also the Schottky contacts (n-type and p type).

To better describe the effect of the electric field on the electronic properties of the G/MoSeS heterostructure, in Fig. 6(c-f) we present the band structures of the G/MoSeS heterostructure under different strengths of the applied electric field. As compared with the band structure of equilibrium G/MoSeS heterostructure (E_{field}) = 0 V/nm), we find that by applying negative electric field the Fermi level shifts upwards from the VBM to CBM of the Janus MoSeS monolayer, resulting in a/an decrease/increase in the n-type/p-type SBH of the G/MoSeS heterostructure, as illustrated in Fig. 6(c). Thus, the G/MoSeS heterostructure still keeps the n-type Schottky contact when negative electric field is applied. When positive electric field is applied, we find that the Fermi level is downshifted from the CBM to VBM of the Janus

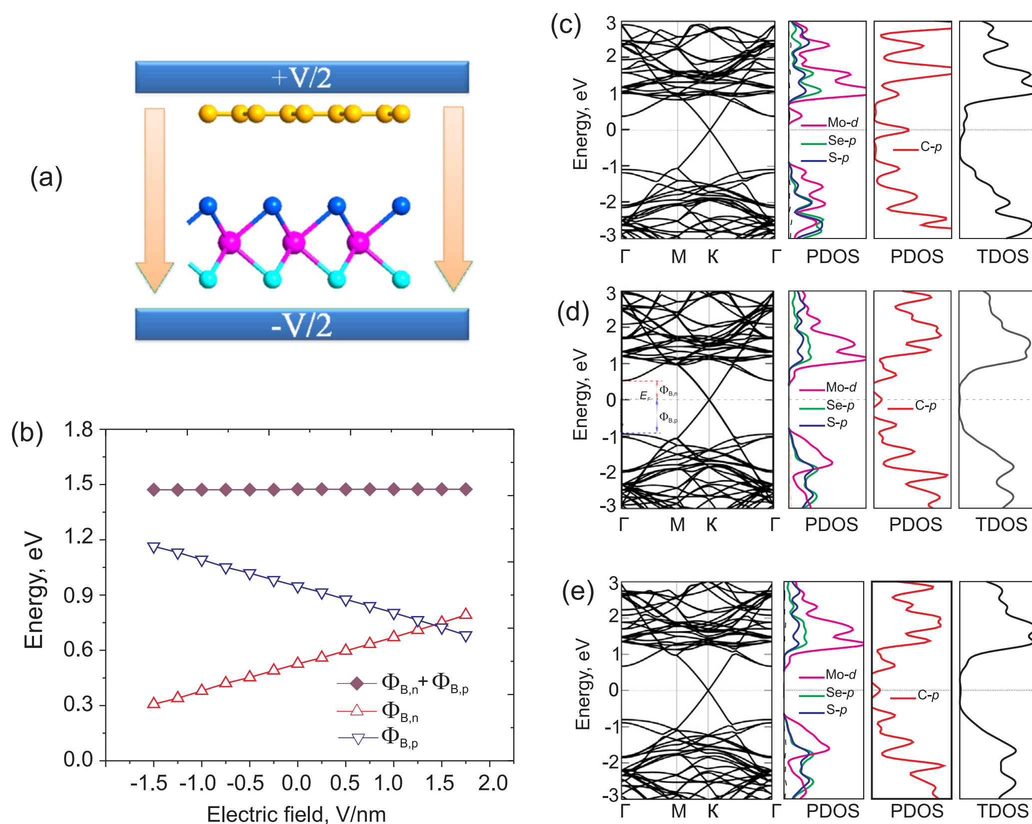

Fig. 6. (a) The schematic diagram of the G/MoSeS heterostructure under applied electric field perpendicularly to the heterostructure; (b) The dependence of the SBH in G/MoSeS heterostructure as a function of E_{field}; The band structures and PDOS of the G/MoSeS heterostructure under different strengths of electric field of (c) −1 V/nm, (d) 0 V/nm, and (e) +1 V/nm, respectively. The Fermi level is set to be zero.

MoSeS monolayer, resulting in an/a increase/decrease in the *n*-type/*p*-type SBH, as shown in Fig. 6(e). When positive electric field is larger than +1.5 V/nm, a transition of the Schottky contact from the *n*-type to the *p*-type was observed in the G/MoSeS heterostructure. The *p*-type SBH under electric field of +1.5 V/nm is 0.72 eV. The transition between the *n*-type and *p*-type Schottky contacts plays an important role in designing the novel Schottky devices based on G/MoSeS heterostructure with the dynamic switching between them. Finally, it should be noted that due to the linear dependence of both the *n*-type and *p*-type SBH on the E_{field}, the *n*-type or *p*-type SBH can be made zero or negative under large E_{field} strength. This zero or negative *n*-type/*p*-type SBH indicates a transformation between the Schottky contact and Ohmic contact in the G/MoSeS heterostructure. However, such large strength of an electric field may not easily be introduced by experiments.

4. Conclusions

In summary, we have systematically investigated the structural and electronic properties of the G/MoSeS and G/MoSSe heterostructures by using density functional theory. The effect of the electric field applied perpendicularly to the surface on the electronic properties and Schottky barrier of the G/MoSeS heterostructure has also been studied. The results show that owing to the weak vdW interaction between the G layer and the Janus MoSeS monolayer, the electronic properties of the G/MoSeS heterostructures are well kept. At the equilibrium state, the interlayer distance between the G layer and the topmost MoSeS layer is 3.34 Å, and the binding energy per carbon atom is −3 meV. Upon contact, graphene becomes a semiconductor with a tiny band gap of 3 meV, making graphene suitable for application in the next generation electronic and optoelectronic devices. Furthermore, the G/MoSeS heterostructure forms an *n*-type Schottky contact with the Schottky barrier height of 0.53 eV at the equilibrium state. Our results also indicate that the electric field applied perpendicularly to the heterostructure could control not only the Schottky barrier height, but also the Schottky contact type from the *n*-type to *p*-type. Based on these extraordinary electronic properties of ultra-thin G/MoSeS heterostructures, which are expected to be with great applications in nanoelectronic and optoelectronic devices in the future experiments.

Acknowledgements

This research is funded by Vietnam National Foundation for Science and Technology Development (NAFOSTED) under Grant No. 103.01-2016.07. B. Amin acknowledges support from the Higher Education Commission of Pakistan (HEC) under Project No. 5727/KPK/NRPU/R&D/HEC2016.

References

[1] K.S. Novoselov, A.K. Geim, S.V. Morozov, D. Jiang, Y. Zhang, S.V. Dubonos, I.V. Grigorieva, A.A. Firsov, Electric field effect in atomically thin carbon films, Science 306 (5696) (2004) 666–669.
[2] Q. Tang, Z. Zhou, Graphene-analogous low-dimensional materials, Prog. Mater. Sci. 58 (8) (2013) 1244–1315.
[3] C.R. Dean, A.F. Young, I. Meric, C. Lee, L. Wang, S. Sorgenfrei, K. Watanabe, T. Taniguchi, P. Kim, K.L. Shepard, et al., Boron nitride substrates for high-quality graphene electronics, Nat. Nanotechnol. 5 (10) (2010) 722–726.
[4] N. Alem, R. Erni, C. Kisielowski, M.D. Rossell, W. Gannett, A. Zettl, Atomically thin hexagonal boron nitride probed by ultrahigh-resolution transmission electron microscopy, Phys. Rev. B 80 (15) (2009) 155425.
[5] K.H. Lee, H.-J. Shin, J. Lee, I.-y. Lee, G.-H. Kim, J.-Y. Choi, S.-W. Kim, Large-scale synthesis of high-quality hexagonal boron nitride nanosheets for large-area graphene electronics, Nano Lett. 12 (2) (2012) 714–718.
[6] Q.H. Wang, K. Kalantar-Zadeh, A. Kis, J.N. Coleman, M.S. Strano, Electronics and optoelectronics of two-dimensional transition metal dichalcogenides, Nat. Nanotechnol. 7 (11) (2012) 699.
[7] M. Chhowalla, H.S. Shin, G. Eda, L.-J. Li, K.P. Loh, H. Zhang, The chemistry of two-dimensional layered transition metal dichalcogenide nanosheets, Nat. Chem. 5 (4)

(2013) 263.
[8] W.S. Yun, S. Han, S.C. Hong, I.G. Kim, J. Lee, Thickness and strain effects on electronic structures of transition metal dichalcogenides: 2H-MX_2 semiconductors (M= Mo, W; X= S, Se, Te), Phys. Rev. B 85 (3) (2012) 033305.
[9] Z. Zhu, Y. Cheng, U. Schwingenschlögl, Giant spin-orbit-induced spin splitting in two-dimensional transition-metal dichalcogenide semiconductors, Phys. Rev. B 84 (15) (2011) 153402.
[10] C.V. Nguyen, N.N. Hieu, N.A. Poklonski, V.V. Ilyasov, L. Dinh, T.C. Phong, L.V. Tung, H.V. Phuc, Magneto-optical transport properties of monolayer MoS_2 on polar substrates, Phys. Rev. B 96 (12) (2017) 125411.
[11] Y. Zhou, Y. Nie, Y. Liu, K. Yan, J. Hong, C. Jin, Y. Zhou, J. Yin, Z. Liu, H. Peng, Epitaxy and photoresponse of two-dimensional GaSe crystals on flexible transparent mica sheets, ACS Nano 8 (2) (2014) 1485–1490.
[12] X. Li, M.-W. Lin, A.A. Puretzky, J.C. Idrobo, C. Ma, M. Chi, M. Yoon, C.M. Rouleau, I.I. Kravchenko, D.B. Geohegan, K. Xiao, Controlled vapor phase growth of single crystalline, two-dimensional gase crystals with high photoresponse, Sci. Rep. 4 (2014) 5497.
[13] Y. Ma, Y. Dai, M. Guo, L. Yu, B. Huang, Tunable electronic and dielectric behavior of gas and gase monolayers, Phys. Chem. Chem. Phys. 15 (19) (2013) 7098–7105.
[14] L. Huang, Z. Chen, J. Li, Effects of strain on the band gap and effective mass in two-dimensional monolayer GaX (X= S, Se, Te), RSC Adv. 5 (8) (2015) 5788–5794.
[15] M. Yagmurcukardes, R. Senger, F. Peeters, H. Sahin, Mechanical properties of monolayer GaS and GaSe crystals, Phys. Rev. B 94 (24) (2016) 245407.
[16] A.-Y. Lu, H. Zhu, J. Xiao, C.-P. Chuu, Y. Han, M.-H. Chiu, C.-C. Cheng, C.-W. Yang, K.-H. Wei, Y. Yang, W. Yuan, S. Dimosthenis, N. Dennis, Y. Peidong, A.M. David, C. Mei-Yin, Z. Xiang, L. Lain-Jong, Janus monolayers of transition metal dichalcogenides, Nat. Nanotechnol. 12 (8) (2017) 744.
[17] J. Zhang, S. Jia, I. Kholmanov, L. Dong, D. Er, W. Chen, H. Guo, Z. Jin, V.B. Shenoy, L. Shi, L. Jun, Janus monolayer transition-metal dichalcogenides, ACS Nano 11 (8) (2017) 8192–8198.
[18] L. Dong, J. Lou, V.B. Shenoy, Large in-plane and vertical piezoelectricity in Janus transition metal dichalchogenides, ACS Nano 11 (8) (2017) 8242–8248.
[19] Y. Ji, M. Yang, H. Lin, T. Hou, L. Wang, Y. Li, S.-T. Lee, Janus structures of transition metal dichalcogenides as the heterojunction photocatalysts for water splitting, J. Phys. Chem. C 122 (2018) 31233129.
[20] F. Li, W. Wei, P. Zhao, B. Huang, Y. Dai, Electronic and optical properties of pristine and vertical and lateral heterostructures of Janus MoSSe and WSSe, J. Phys. Chem. Lett. 8 (23) (2017) 5959–5965.
[21] S.-D. Guo, Biaxial strain tuned electronic structures and power factor in Janus transition metal dichalchogenide monolayers. Available from: arXiv preprint < arXiv:1803.04147 > .
[22] Z. Guan, S. Ni, S. Hu, Tunable electronic and optical properties of monolayer and multilayer Janus Mosse as a photocatalyst for solar water splitting: a first-principles study, J. Phys. Chem. C 122 (2018) 62096216.
[23] Y. Sata, R. Moriya, S. Morikawa, N. Yabuki, S. Masubuchi, T. Machida, Electric field modulation of Schottky barrier height in graphene/$MoSe_2$ van der Waals hetero-interface, Appl. Phys. Lett. 107 (2) (2015) 023109.
[24] F. Zhang, W. Li, Y. Ma, Y. Tang, X. Dai, Tuning the Schottky contacts at the graphene/WS_2 interface by electric field, RSC Adv. 7 (47) (2017) 29350–29356.
[25] Z. Guan, S. Ni, S. Hu, Band gap opening of graphene by forming a graphene/$PtSe_2$ van der Waals heterojunction, RSC Adv. 7 (72) (2017) 45393–45399.
[26] R. Lu, J. Liu, H. Luo, V. Chikan, J.Z. Wu, Graphene/GaSe-nanosheet hybrid: towards high gain and fast photoresponse, Sci. Rep. 6 (2016) 19161.
[27] W. Kim, C. Li, F.A. Chaves, D. Jiménez, R.D. Rodriguez, J. Susoma, M.A. Fenner, H. Lipsanen, J. Riikonen, Tunable graphene–GaSe dual heterojunction device, Adv. Mater. 28 (9) (2016) 1845–1852.
[28] B. Cho, J. Yoon, S.K. Lim, A.R. Kim, D.-H. Kim, S.-G. Park, J.-D. Kwon, Y.-J. Lee, K.-H. Lee, B.H. Lee, H.C. Ko, M.G.H. Hahm, Chemical sensing of 2D graphene/MoS_2 heterostructure device, ACS Appl. Mater. Interfaces 7 (30) (2015) 16775–16780.
[29] H. Tian, Z. Tan, C. Wu, X. Wang, M.A. Mohammad, D. Xie, Y. Yang, J. Wang, L.-J. Li, J. Xu, T.-L. Ren, Novel field-effect Schottky barrier transistors based on graphene-MoS_2 heterojunctions, Sci. Rep. 4 (2014) 5951.
[30] H. Xu, J. Wu, Q. Feng, N. Mao, C. Wang, J. Zhang, High responsivity and gate tunable graphene-MoS_2 hybrid phototransistor, Small 10 (11) (2014) 2300–2306.
[31] T. Georgiou, R. Jalil, B.D. Belle, L. Britnell, R.V. Gorbachev, S.V. Morozov, Y.-J. Kim, A. Gholinia, S.J. Haigh, O. Makarovsky, L. Eaves, L.A. Ponomarenko, A.K. Geim, K.S. Novoselov, A. Mishchenko, Vertical field-effect transistor based on graphene-WS_2 heterostructures for flexible and transparent electronics, Nat. Nanotechnol. 8 (2) (2013) 100.
[32] Y. Ma, Y. Dai, M. Guo, C. Niu, B. Huang, Graphene adhesion on MoS_2 monolayer: an ab initio study, Nanoscale 3 (9) (2011) 3883–3887.
[33] C.V. Nguyen, Tuning the electronic properties and Schottky barrier height of the vertical graphene/MoS_2 heterostructure by an electric gating, Superlattices Microstruct. 116 (2018) 79–87.
[34] L. Yu, Y.-H. Lee, X. Ling, E.J. Santos, Y.C. Shin, Y. Lin, M. Dubey, E. Kaxiras, J. Kong, H. Wang, et al., Graphene/MoS_2 hybrid technology for large-scale two-dimensional electronics, Nano Lett. 14 (6) (2014) 3055–3063.
[35] J.A. Miwa, M. Dendzik, S.S. Grønborg, M. Bianchi, J.V. Lauritsen, P. Hofmann, S. Ulstrup, Van der Waals epitaxy of two-dimensional MoS_2–graphene heterostructures in ultrahigh vacuum, Acs Nano 9 (6) (2015) 6502–6510.
[36] N.N. Hieu, H.V. Phuc, V.V. Ilyasov, N.D. Chien, N.A. Poklonski, N. Van Hieu, C.V. Nguyen, First-principles study of the structural and electronic properties of graphene/MoS_2 interfaces, J. Appl. Phys. 122 (10) (2017) 104301.
[37] Y. Ma, Y. Dai, W. Wei, C. Niu, L. Yu, B. Huang, First-principles study of the Graphene@$MoSe_2$ heterobilayers, J. Phys. Chem. C 115 (41) (2011) 20237–20241.
[38] Y. Hong, M.G. Ju, J. Zhang, X.C. Zeng, Phonon thermal transport in a graphene/$MoSe_2$ van der Waals heterobilayer, Phys. Chem. Chem. Phys. 20 (2018) 2637.
[39] C. Zheng, Q. Zhang, B. Weber, H. Ilatikhameneh, F. Chen, H. Sahasrabudhe, R. Rahman, S. Li, Z. Chen, J. Hellerstedt, Y. Zhang, W.D. Hui, Q. Bao, M.S. Fuhrer, Direct observation of 2d electrostatics and ohmic contacts in template-grown graphene/WS_2 heterostructures, ACS Nano 11 (3) (2017) 2785–2793.
[40] A. Azizi, S. Eichfeld, G. Geschwind, K. Zhang, B. Jiang, D. Mukherjee, L. Hossain, A.F. Piasecki, B. Kabius, J.A. Robinson, N. Alem, Freestanding van der Waals heterostructures of graphene and transition metal dichalcogenides, ACS Nano 9 (5) (2015) 4882–4890.
[41] J. Shim, H.S. Kim, Y.S. Shim, D.-H. Kang, H.-Y. Park, J. Lee, J. Jeon, S.J. Jung, Y.J. Song, W.-S. Jung, J. Lee, S. Park, J. Kim, S. Lee, Y.-H. Kim, J.-H. Park, Extremely large gate modulation in vertical graphene/WSe_2 heterojunction barristor based on a novel transport mechanism, Adv. Mater. 28 (26) (2016) 5293–5299.
[42] K. Kim, S. Larentis, B. Fallahazad, K. Lee, J. Xue, D.C. Dillen, C.M. Corbet, E. Tutuc, Band alignment in WSe_2–graphene heterostructures, ACS Nano 9 (4) (2015) 4527–4532.
[43] Z.G. Yu, Y.-W. Zhang, B.I. Yakobson, Strain-robust and electric field tunable band alignments in van der Waals WSe_2–graphene heterojunctions, J. Phys. Chem. C 120 (39) (2016) 22702–22709.
[44] P. Giannozzi, S. Baroni, N. Bonini, M. Calandra, R. Car, C. Cavazzoni, D. Ceresoli, G.L. Chiarotti, M. Cococcioni, I. Dabo, et al., Quantum espresso: a modular and open-source software project for quantum simulations of materials, J. Phys.: Condens. Matter 21 (39) (2009) 395502.
[45] J.P. Perdew, K. Burke, M. Ernzerhof, Generalized gradient approximation made simple, Phys. Rev. Lett. 77 (18) (1996) 3865.
[46] J.P. Perdew, J.A. Chevary, S.H. Vosko, K.A. Jackson, M.R. Pederson, D.J. Singh, C. Fiolhais, Atoms, molecules, solids, and surfaces: applications of the generalized gradient approximation for exchange and correlation, Phys. Rev. B 46 (11) (1992) 6671.
[47] J. Perdew, K. Burke, M. Ernzerhof, Perdew, Burke, and Ernzerhof reply, Phys. Rev. Lett. 80 (4) (1998) 891.
[48] P.E. Blöchl, Projector augmented-wave method, Phys. Rev. B 50 (24) (1994) 17953.
[49] S. Grimme, Semiempirical gga-type density functional constructed with a long-range dispersion correction, J. Comput. Chem. 27 (15) (2006) 1787–1799.
[50] M. Sun, J.-P. Chou, J. Yu, W. Tang, Effects of structural imperfection on the electronic properties of graphene/WSe_2 heterostructures, J. Mater. Chem. C 5 (39) (2017) 10383–10390.
[51] W. Tang, M. Sun, J. Yu, J.-P. Chou, Magnetism in non-metal atoms adsorbed graphene-like gallium nitride monolayers, Appl. Surf. Sci. 427 (2018) 609–612.
[52] J. Bardeen, Surface states and rectification at a metal semi-conductor contact, Phys. Rev. 71 (1947) 717–727.
[53] W. Chen, E.J. Santos, W. Zhu, E. Kaxiras, Z. Zhang, Tuning the electronic and chemical properties of monolayer MoS_2 adsorbed on transition metal substrates, Nano Lett. 13 (2) (2013) 509–514.
[54] W. Hu, T. Wang, R. Zhang, J. Yang, Effects of interlayer coupling and electric fields on the electronic structures of graphene and MoS_2 heterobilayers, J. Mater. Chem. C 4 (9) (2016) 1776–1781.
[55] M. Sun, J.-P. Chou, Q. Ren, Y. Zhao, J. Yu, W. Tang, Tunable Schottky barrier in van der Waals heterostructures of graphene and g-GaN, Appl. Phys. Lett. 110 (17) (2017) 173105.
[56] J. Padilha, A. Fazzio, A.J. da Silva, van der Waals heterostructure of phosphorene and graphene: tuning the Schottky barrier and doping by electrostatic gating, Phys. Rev. Lett. 114 (6) (2015) 066803.
[57] H.V. Phuc, V.V. Ilyasov, N.N. Hieu, B. Amin, C.V. Nguyen, Van der Waals graphene/g-GaSe heterostructure: tuning the electronic properties and Schottky barrier by interlayer coupling, biaxial strain, and electric gating, J. Alloys Compd. 750 (2018) 765–773.
[58] H.V. Phuc, N.N. Hieu, B.D. Hoi, L.T. Phuong, N.V. Hieu, C.V. Nguyen, Out-of-plane strain and electric field tunable electronic properties and Schottky contact of graphene/antimonene heterostructure, Superlattices Microstruct. 112 (2017) 554–560.
[59] J. Kang, W. Liu, D. Sarkar, D. Jena, K. Banerjee, Computational study of metal contacts to monolayer transition-metal dichalcogenide semiconductors, Phys. Rev. X 4 (3) (2014) 031005.
[60] H. Wang, C. Si, J. Zhou, Z. Sun, Vanishing Schottky barriers in blue phosphorene/mxene heterojunctions, J. Phys. Chem. C 121 (45) (2017) 25164–25171.
[61] M. Farmanbar, G. Brocks, Ohmic contacts to 2d semiconductors through van der Waals bonding, Adv. Electron. Mater. 2 (4) (2016) 1600318.